First field evidence of coseismic land-level change associated with the 25th December 2016 M_w 7.6 Chiloé earthquake, Chile

Ed Garrett*, Martin Brader, Daniel Melnick, Jonathan Bedford and Diego Aedo

* Department of Geography, Durham University, South Road, Durham, DH1 3LE, United Kingdom

Abstract

Assessments of megathrust earthquake rupture patterns provide fundamental insights into the processes that control the seismic cycle along subduction zones. When large earthquakes occur in regions with sparse geodetic networks, as was the case for the magnitude (M_w) 7.6 Chiloé, Chile earthquake of 25th December 2016, estimates of vertical coseismic deformation from fixed intertidal biotic indicators provide important evidence that helps to constrain fault slip. Ten months after the Chiloé earthquake we observed a white fringe of bleached coralline algae (Corallinaceae) along the southeastern coastline of Isla Quilán, south of Isla de Chiloé, killed by reduced tidal wetting resulting from coseismic land uplift. Our quantitative measurements of the vertical extent of algal mortality provide the first field-based report of the effects of the 2016 earthquake. We infer Isla Quilán coseismically uplifted by 25.8 ± 14.3 cm. The vertical extent of mortality and the aspect (compass direction) of the bedrock surface are uncorrelated, but we find that exposure to waves and shielding from insolation may prevent or delay

mortality. Focusing on sites sheltered from waves, we demonstrate that with a large number of measurements (> 100), land-level changes as low as 25 cm may be quantitatively assessed. The absence of bleaching on Isla de Chiloé may reflect the smaller magnitude of coseismic uplift at this location or the lack of suitably sheltered bedrock surfaces. Previously published fault dislocation models are consistent with our field observations; however, the coralline algae data are on their own insufficient to discriminate between competing hypotheses over the amount of fault slip. By combining our field data with space geodetic data in a model that uses detailed fault geometry, we constrain peak slip to ~3 m, approximately 80% of the maximum cumulative plate convergence since the last great earthquake in the region.

Introduction

Assessing the slip distribution of megathrust earthquakes is fundamental to gain insight into the processes that control the seismic cycle. When megathrust earthquakes occur in regions with sparse geodetic networks, estimates of vertical coseismic deformation from fixed intertidal biotic indicators help to constrain slip magnitudes and distributions (e.g. Plafker, 1965; Bodin and Klinger, 1986; Melnick et al., 2012; Jaramillo et al., 2012; Haeussler et al., 2015). Even in areas with substantial geodetic coverage, uplift measurements based on biotic markers provide independent corroborative data at higher spatial densities than GPS stations (e.g. Awata et al., 2008; Clark et al., 2017). The magnitude (M_w) 7.6 Chiloé earthquake (Fig. 1) ruptured the boundary between the Nazca and South American plates in the vicinity of the remote southern coast of Isla de Chiloé (~43.5°S), ending a period of seismic quiescence in the region stretching

45 back to the 1960 M_w 9.5 Valdivia earthquake, the largest instrumentally recorded earthquake
46 globally. Inversion of seismic and InSAR data provided initial outlines of the characteristics of
47 the rupture, notably suggesting that the maximum coseismic slip of up to 5 m exceeded the slip
48 deficit accumulated since 1960 (Lange et al., 2017; Melgar et al., 2017; Ruiz et al., 2017; Xu,
49 2017). Subsequent integration of deformation recorded by continuous Global Positioning
50 System (GPS) stations – three within 100 km of the epicenter, but none overlying the rupture –
51 suggested a lower maximum slip of ~2.9 m (Moreno et al., 2018). Nearfield observations from
52 the epicentral region are critical for ground truthing these findings. The remote and
53 predominantly offshore location of the rupture zone and the lack of a dense proximal geodetic
54 network (Fig. 1) serve to increase the importance of such observations.
55
56 In this paper, we focus on quantitative estimates of coseismic land-level change provided by
57 observations of sessile intertidal organisms. The use of fixed intertidal biota to determine the
58 magnitude of abrupt vertical deformation is long established, with members of the 19th century
59 HMS Beagle expedition having measured the > 2 m width of a band of coseismically stranded
60 mussels to assess the uplift of Isla Santa María during the M > 8.5 1835 Chilean earthquake
61 (FitzRoy, 1839; Darwin, 1851). Increasingly systematic approaches employed a range of
62 intertidal flora and fauna to provide high-resolution reconstructions of abrupt changes in land
63 level resulting from earthquakes (e.g. Tarr and Martin, 1912; Plafker, 1969; Plafker and Ward,
64 1992; Carver et al., 1994; Meltzner et al., 2010; Jaramillo et al., 2017). Here we focus on
65 coralline algae, encrusting calcareous algae of the family Corallinaceae, found at the lower
66 limits of the intertidal range and subtidally within the photic zone (Ortlieb et al., 1996). Our

quantitative measurements of algal mortality provide the first field-based report of the effects of the 2016 earthquake. We seek to use our field observations to inform the debate over whether coseismic slip exceeded the post-1960 slip deficit and to understand the role of the 2016 earthquake within the seismic cycle of the Chilean megathrust.

Tectonic setting and the 2016 earthquake

The convergence of the Nazca and South American plates, at a rate of 66 mm yr^{-1} (Angermann et al., 1999), drives the seismicity of the Chilean megathrust. Prior to the 2016 earthquake, the 1960 M_w 9.5 Valdivia rupture extended over an along-strike distance of ~ 1000 km (Plafker and Savage, 1970), defining the extent of the Valdivia seismic segment (Fig. 1a). Moreno et al. (2009) inverted field estimates of coastal emergence and submergence derived by Plafker and Savage (1970) together with resurveyed triangulations and leveling lines to infer the distribution of slip in 1960, obtaining slip exceeding 25 m at the latitude of Isla Guafo, immediately southwest of Isla de Chiloé. GPS velocities collected between 2002 and 2009 suggest spatially heterogeneous post-1960 locking (Moreno et al., 2011) with four highly locked regions distributed over the ~1000-km-long rupture including an area with a radius of approximately 50 km around Isla Guafo (43.6°S). The coincidence of this locked patch with the occurrence of high slip in 1960 suggests this asperity may be a persistent feature over several earthquake cycles (Moreno et al., 2011).

The 2016 Chiloé earthquake occurred on the northeastern, down-dip flank of the interseismically locked Guafo patch, beneath the southern coast of Isla de Chiloé (Fig. 1b). Propagating from ~15 km depth to the intersection between the subducting plate and the continental Moho (~30 km), the rupture was confined to an area of approximately 15 – 20 km radius within the main seismogenic zone (Ruiz et al., 2017; Moreno et al., 2018). A lack of slip at shallow depths (seismogenic failure domains A and partly B, cf. Fig. 15 in Lay et al., 2012) precluded the generation of a tsunami; only small waves (< 20 cm) were observed instrumentally. Inversions of geodetic and teleseismic data suggest peak slip between 2.9 m (Moreno et al., 2018) and 5.0 m (Melgar et al., 2017), potentially exceeding the maximum accumulated slip deficit of ~ 3.7 m implied by assuming full interseismic locking since 1960.

The area north of the 1960 Valdivia rupture zone was affected by the 2010 Maule earthquake (M 8.8) which had a rupture length of ~500 km (Moreno et al., 2012). An analysis of surface displacements using continuous GPS stations spanning ~1000 km around the 2010 rupture shows an asymmetric rotation pattern and accelerated inland motion in two regions (Melnick et al., 2017). These two regions coincided with locations of the 2015 Illapel (M_w 8.3, 30-32°S) and 2016 Chiloé earthquakes (Fig. 1a), leading to Melnick et al.'s (2017) interpretation that the 2010 earthquake caused increased plate locking in these two regions during a superinterseismic phase.

Study location

Our investigations focus on the southern coastline of Isla de Chiloé and the southeast of Isla Quilán (also known as Guapiquilán) (Fig. 2). Paleozoic and early Triassic metamorphic rocks form the majority of central and southern Chiloé, with Tertiary volcanism locally exposed on Isla Quilán (Muñoz et al., 2000; Duhart and Adriasola, 2008). The shorelines of southeastern Isla Quilán and the adjacent Isla Refugio possess exposed bedrock headlands and widespread sand, gravel or boulder beaches (Fig. 2b). Adjacent to the settlement of Inio, the Río Inio estuary marks a center of Holocene fine-grained sedimentary accumulation. The rocky headland of Punta Rocosa lies at the mouth of the estuary (Fig. 2c). The remote location and very difficult access for much of the coastline prevented us from surveying other areas of southern Chiloé. The region of interest is microtidal, with a modeled great diurnal range of 1.56 m at Isla Quilán and 1.70 m at Punta Rocosa (Egbert and Erofeeva, 2002).

The bedrock outcrops and boulder accumulations around Isla Quilán and Punta Rocosa provide suitable environments for the development of sessile biotic communities. While little published work relates to the southern coast of Chiloé, Velásquez et al. (2016) describe intertidal biota from analogous sites in northern Chiloé, 140 to 180 km north of the sites investigated in this paper. They report 16 sessile taxa, but do not attempt to subdivide crustose coralline algae into different genera. Velásquez et al. (2016) report the greatest abundances of coralline algae – up to 100 % coverage – in the lower-middle and lower quartiles of the intertidal range. Co-occurring sessile taxa in the low intertidal zone include the cholorophyte *Codium dimorphum*, the branched coralline algae *Corallina officinalis* and the phaeophytes *Durvillaea antarctica* and *Lessonia spicata*.

The southern coastline of Chiloé lies within the zone of coseismic subsidence during the 1960 Valdivia earthquake (Fig. 1a). Comparison of the pre- and post-earthquake lower growth limits of terrestrial vegetation suggest subsidence of 2.1 ± 0.2 m at the Quilanlar estuary, approximately 5 km east of Inio (Plafker and Savage, 1970). We observed ghost forests of dead but standing trees in locations now occupied by tidal marsh, tidal flat or beach environments in the Inio estuary and on Isla Quilán, which we interpret as evidence of substantial relative sea-level rise associated with coseismic subsidence in 1960. The living counterparts, a mixture of *Podocarpus nubigena*, *Sophora cassioides*, *Nothofagus dombeyi* and species of the Myrtaceae family, are found above the highest reaches of current tides.

Field approach

Lying above the rupture zone of the 2016 earthquake, southern Isla de Chiloé experienced coseismic vertical deformation on a centimeter to decimeter scale (Fig. 2a) (Lange et al., 2017; Melgar et al., 2017; Ruiz et al., 2017; Xu, 2017). Coseismic uplift and subsidence are experienced along coastlines as abrupt decreases or increases in relative sea level. The direction, magnitude and spatial pattern of these sea-level changes largely reflects the amount and distribution of slip on the fault (Thatcher, 1984; Nelson, 2007; Shennan et al., 2016). As the distribution of many sessile intertidal organisms along rocky coastlines closely reflects certain tidal levels, they may be used as precise and reliable indicators of current and past sea levels (Laborel and Laborel-Deguen, 1996; Laborel, 2005; Rovere et al., 2015). Approaches for

154 estimating coseismic uplift using sessile species predominantly focus on changes in the lethal
155 limit, the elevation of the upper growth boundary above which the particular organism cannot
156 survive (Kaye, 1964). When coseismically uplifted, organisms are raised above the lethal limit,
157 resulting in mortality. The magnitude of uplift can consequently be derived simply through
158 measuring the vertical extent of mortality (VEM), the difference in the upper limit of the dead
159 organism and the upper limit of the living, post-earthquake counterpart (Bodin and Klinger,
160 1986; Carver et al., 1994).
161
162 Our field investigations, undertaken during low tides in August and October 2017, focused on
163 identifying the upper limits of pre- and post-earthquake coralline algae to establish the VEM.
164 The crustose or rock-encrusting forms of these calcareous red algae are widely distributed
165 around the world, occurring from the lower limits of the intertidal zone down to the limit of the
166 photic zone (Adey and Macintyre, 1973; Lagabrielle et al., 2003). Their lethal limit is controlled
167 by tidal inundation, with desiccation, elevated temperatures and solar radiation resulting in the
168 mortality of colonies that are exposed above water level for more than a few hours (Ortlieb et
169 al., 1996; Martone et al., 2010). Mortality is accompanied by a characteristic color change from
170 pink, purple or light brown to white, with the bleached white colonies conspicuous for months
171 after the bleaching event (e.g. Bodin and Klinger, 1986; Ramirez-Herrera and Orozco, 2002). The
172 dead algae may be eroded over time by wave action, leading to underestimation of the
173 magnitude of uplift if VEM measurements are not completed within months of the earthquake
174 (Lagabrielle et al., 2003). Postseismic deformation may also influence the distribution of the
175 living post-earthquake algae, with subsidence allowing recolonisation of the lower margin of

the bleached zone, further supporting the need for rapid assessments (Ramirez-Herrera and Orozco, 2002).

Our investigations of coralline algae in south central Chile follow their successful application for estimating coastal uplift associated with the 1995 Antofagasta earthquake (Ortlieb et al., 1996), the 2010 Maule earthquake (Castilla et al., 2010; Farias et al., 2010; Vargas et al., 2011) and the 2014 Iquique earthquake (Jaramillo et al., 2017) in northern and central Chile. Ortlieb et al. (1996) and Vargas et al. (2011) note that the VEM is typically greater in locations more exposed to wave splash. Furthermore, uncertainty estimates are also greater for more exposed locations due to greater variability in the measured VEM (Vargas et al., 2011). Vargas et al. (2011) suggest uncertainties of ± 10 – 20 cm for sheltered sites and ± 20 – 60 cm for areas highly exposed to waves. For each sampling site, we made a qualitative judgement on whether the site was sheltered, moderately exposed or highly exposed to waves. We limited our measurements to bedrock sites with largely parallel limits of the bleached and living algae colonies, avoiding detached blocks that could have moved during the earthquake. We also avoided areas with ponded water that might reduce or prevent desiccation. Cracks may enable wicking of water to higher elevations (Haeussler et al., 2015), allowing isolated algae patches to survive at elevations above the main zone of encrustation. We avoided measuring these isolated patches, but note that the conglomeritic nature of the bedrock and the lack of smooth surfaces result in a degree of variability in the elevation of the upper limits of dead and living algae. By taking repeated VEM measurements at a horizontal spacing of 20 – 50 cm at sites with clearly defined limits, we sought to reduce this uncertainty.

Following Ramirez-Herrera and Orozco (2002) we measured the VEM along vertical surfaces using a tape measure. We report our measurements at the centimeter scale; however, the use of a tape measure introduces a small but unquantified uncertainty. Nevertheless, we assume that this uncertainty is not significant in comparison to the variability in the growth limits of the algae and in the consequent VEM. We report concurrent measurements of the aspect of the bedrock surface to the closest 10°.

While Lemoine (1913, 1920) described four species from Isla de Chiloé, due to limited taxonomic analyses and difficulties in identification in the field (Meneses, 1993; Ortlieb et al., 1996; Castilla et al., 2010; Velásquez et al., 2016), we do not attempt to classify the coralline algae encountered.

Survey results

We observed a laterally discontinuous band of bleached coralline algae visible at low tide during our two visits to Isla Quilán, eight and ten months after the 2016 Chiloé earthquake (Figs. 2b, 3a, 3b). Living algae at lower elevations beneath this white band retained their living brown or pink hue (Fig. 3c). During our second visit, in October 2017, we measured the vertical extent of mortality 103 times at five discrete but closely spaced sites in the southeast of Isla Quilán or the western coast of Isla Refugio (Fig. 2b, sites 1, 2, 4, 5 and 6). We noted the presence or absence of bleaching at a further seven sites on Isla Quilán (Fig. 2b, sites 3a, 3b, 3c,

7, 8, 9 and 10) and three more sites around Punta Rocosa at the mouth of the Inio estuary (Fig. 2c, sites 11, 12 and 13).

The mean VEM at the five Isla Quilán measurement sites ranged from 23.3 cm to 28.7 cm (Table 1). The mean of all 103 VEM measurements (±2σ) was 25.8 ± 14.3 cm, with the data displaying a Gaussian distribution (Fig. 4a). At sites 3b, 3c, 7, 8 and 10 we observed bleaching but could not quantify the extent of mortality. Sites 3b, 3c, 8 and 10 lacked vertically inclined bedrock surfaces where accurate measurements could be made; however, we observed bleaching on both subhorizontal bedrock outcrops and rounded boulders (Fig. 3e). Site 7 displayed bleached algae, but lacked clearly identifiable living algae, preventing us from ascertaining the post-earthquake lethal limit.

We observed or measured bleaching at most aspects on Isla Quilán, with a notable exception between 150° and 210° (Fig. 4b). We do not find any relationship between the VEM and the aspect of the bedrock surface for aspects from 330° through to 90° (r^2 = 0.001; n = 100). Two moderately exposed south-facing sites on Isla Quilán (Fig. 2b, sites 3a, 9) displayed no bleaching, with pigmented and therefore presumably living algae at the highest extent of coralline algal growth (Fig. 3d). We did not observe any bleached algae at the three moderately or highly exposed sites around Punta Rocosa (Fig. 2c, Fig. 3f). These sites also share predominantly southerly aspects of 140 – 200°.

Thresholds of evidence creation and preservation

242

243 The absence of bleaching at sites 3a and 9 on Isla Quilán (Fig. 2b), despite the occurrence of
244 bleaching at adjacent sites assumed to have experienced a similar magnitude of uplift, implies
245 the existence of a threshold for bleaching that is not solely dependent on elevation with respect
246 to the tidal frame. The two unbleached sites on Isla Quilán are moderately exposed to wave
247 splash and we propose that the combined effects of shielding from solar radiation due to their
248 southern aspect, overhanging vegetation and continued wetting may have prevented or
249 delayed algal mortality. While these environmental factors may exert a control on the presence
250 or absence of bleaching, the extent to which they individually or in conjunction influence the
251 magnitude of the VEM remains unclear. Our hypothesis that increased wave splash may
252 contribute to preventing or delaying bleaching contrasts with previous investigations that
253 suggest the VEM increases with increasing wave exposure (Ortlieb et al., 1996; Vargas et al.,
254 2010), highlighting the need for further comprehensive assessments of the environmental
255 controls on coralline algae bleaching.

256

257 Lagabrielle et al. (2003) highlight that subaerial erosion of the uppermost colonies of bleached
258 algae may, over time, reduce the observed VEM. Their study of algae uplifted by the M_w 7.5
259 1999 Ambrym earthquake, Vanuatu, notes lowering of the upper limit of bleached algae by
260 several decimeters over 26 months following the earthquake, with near complete loss in some
261 areas. We did not observe any evidence for erosion of bleached algae 10 months after the 2016
262 Chiloé earthquake, with algae at the upper limit having been partially colonized by
263 chlorophytes, but otherwise appearing intact and undamaged.

Postseismic deformation may influence the preservation of the magnitude of the coseismic uplift signal. Continued postseismic uplift may increase the VEM, while subsidence may allow recolonisation of the lower margin of the bleached zone. Inverse modeling suggests maximum pre-earthquake interseismic uplift rates of 10 mm yr^{-1} at Isla Quilán (Melnick et al., in press). The extent to which this rate changed following the earthquake is unclear; however, earthquakes rupturing the deeper regions of the seismogenic zone have been characterized by short, low amplitude postseismic deformation (e.g. Béjar-Pizarro et al., 2010; Melgar et al., 2017). Therefore, the amplitude of postseismic deformation and the influence on the observed VEM might be limited. At Quellón (Fig. 1b), 70 mm of coseismic subsidence in 2016 was followed by 30 mm of postseismic uplift by October 2017 (Fig. 5). If Isla Quilán also experienced a reversal of the coseismic motion during the postseismic period, our VEM measurements may underestimate the magnitude of coseismic uplift due to subsequent subsidence. Nevertheless, if postseismic uplift at Quellón reflects afterslip down-dip of the mainshock, Isla Quilán may have experienced a smaller magnitude of postseismic subsidence, or continued uplift. As we currently have no further constraints on the postseismic deformation rate or direction, we cannot apply any straightforward correction to our VEM-based estimate of uplift.

Comparison with slip models

The vertical extent of coralline algae mortality suggests the 2016 Chiloé earthquake uplifted southeastern Isla Quilán by 25.8 ± 14.3 cm. In Figure 6 we compare this estimate with the

vertical deformation predicted by dislocation models featuring either restricted peak slip (Moreno et al., 2018) or peak slip exceeding the accumulated post-1960 slip deficit (Lange et al., 2017). We project the Lange et al. (2017) slip distribution onto the more realistic, three dimensional and undulating fault geometry of Moreno et al. (2018) to eliminate differences in surface deformation predictions resulting from this factor. This interpolation reduces the maximum slip in the Lange et al. (2017) model from 4.2 m to 3.8 m, closer to the 3.7 m deficit implied by full locking, but still greater than the deficit that would be associated with incomplete or delayed post-1960 locking (Moreno et al., 2011). Our field observations are consistent with either model, with both predicting uplift of between 20 and 35 cm at Isla Quilán. Predictions from both models highlight maximum uplift occurring trenchward, either ~10 or ~30 km west of Isla Quilán (Fig. 2a).

The lack of bleaching observed at Punta Rocosa suggests any coseismic uplift at this location did not exceed the evidence creation threshold. Our interpretation of the Isla Quilán observations suggests moderately exposed, south-facing colonies may remain unbleached even in the event of uplift of ~25 cm. As the Punta Rocosa sites are predominantly south facing and are moderately or highly exposed, we cannot rule out a small amount of uplift. Furthermore, Vargas et al. (2011) propose uncertainties in excess of ± 20 cm for areas highly exposed to waves, providing additional evidence that these sites are not suited to recording centimeter-scale deformation. The models of both Lange et al. (2017) and Moreno et al. (2018) predict the hingeline between regions of uplift and subsidence lies to the east of Punta Rocosa, with the site having experienced uplift of 5 to 15 cm (Fig. 6).

Incorporating field data into models of coseismic slip

As our field observations are alone insufficient to discriminate between different slip models, we combine them with space-based geodetic data to constrain the distribution and magnitude of slip on the subduction interface. As the initial GPS and InSAR-based model of Moreno et al. (2018) predicts a similar magnitude of uplift at Isla Quilán to our VEM observations, incorporating and upweighting the VEM estimate as an additional constraint does not result in any appreciable revision to this slip model (Fig. 7). Joint inversion of coralline algae, GPS and InSAR data indicates the rupture of a single asperity beneath the southern coast of Isla de Chiloé with maximum slip of ~3 m. Peak slip remains within 5 % of 3 m as the coralline algae data are progressively more heavily weighted (Fig. 7). The heaviest weighting requires a modest (<0.5 m) increase in slip to the southwest of Isla Quilán and a decrease in slip beneath and to the southeast of the island (Fig. 7c).

Discussion and conclusions

Our field observations of sessile intertidal biota ground-truth the amount of coseismic vertical deformation during the 2016 Chiloé earthquake. We interpret measurements of the vertical extent of mortality of crustose coralline algae to indicate Isla Quilán uplifted 25.8 ± 14.3 cm. We find no correlation between the VEM and the aspect of the bedrock surface, but note that exposure to waves and shielding from insolation due to aspect or overhanging vegetation may

prevent or delay mortality. The lack of observed bleaching at Punta Rocosa on Isla de Chiloé may reflect the smaller magnitude of coseismic uplift and the lack of suitably sheltered sites. We find close agreement between our uplift estimate and the predictions of slip models developed using space-based geodetic and seismological approaches (Lange et al., 2017; Moreno et al., 2018). The agreement between our data and the modeling approaches provides further support for several aspects of this event previously noted by other authors. The Chiloé earthquake ruptured the deeper portion of the megathrust (Melgar et al., 2017; Ruiz et al., 2017; Xu, 2017; Moreno et al., 2018), occurring towards the downdip limit of a previously identified region of high interseismic locking (Moreno et al., 2011) and rerupturing an area that had experienced substantial coseismic slip (>10 m) in 1960 (Moreno et al., 2009). Rupture of the deeper regions of the interface (> 15 km) may reflect interseismic loading of this region by the strongly coupled shallower asperity (Moreno et al., 2018).

While earlier rupture models suggest coseismic slip in 2016 was greater than the ~3.7 m slip deficit accumulated since 1960 under the assumption of persistent decadal full locking (Lange et al., 2017; Melgar et al., 2017; Ruiz et al., 2017; Xu, 2017), subsequent modeling implies lower peak slip and does not require exceedance of the slip deficit (Moreno et al., 2018). Our incorporation of a coralline algae-based uplift estimate into the Moreno et al. (2018) model does not change this conclusion. Our modeled maximum slip of ~3 m constitutes approximately 80 % of the cumulative plate convergence since the 1960 earthquake and would therefore be consistent with the release of all of the accumulated strain if plate coupling averaged 80 % over this period. Nevertheless, we stress that the amount of coralline algae bleaching observed at

352 Isla Quilán does not, in itself, preclude higher slip magnitudes and that these are a product of
353 Moreno et al.'s (2018) fault geometry and geodetic data. Models incorporating peak slip in
354 excess of the maximum slip deficit also predict surface displacements within the uncertainty of
355 our field observations (Lange et al., 2017).
356
357 Our survey of coralline algae killed as a result of uplift during the 2016 Chiloé earthquake
358 highlights the utility of these sessile intertidal organisms for providing quantitative coseismic
359 deformation estimates in the absence of other nearfield geodetic data. Our survey results and
360 comparisons with published models demonstrate that with a large number of measurements
361 (> 100) from closely spaced sites, land-level changes as low as 25 cm may be quantitatively
362 assessed. While sheltered sites provide consistent VEM estimates, the influence of wave splash
363 on more exposed sites remains equivocal and further work is needed to evaluate the relative
364 importance of a range of environmental controls on coralline algae mortality in these
365 situations.

Data and resources

Observation of the tsunami wave height on 25th December 2016 is from the Puerto Melinka tide gauge, maintained by the Servicio Hidrográfico y Oceanográfico de la Armada de Chile and accessed via http://www.ioc-sealevelmonitoring.org/station.php?code=pmel. GPS displacements in Fig. 1 are from Moreno et al. (2018) and GPS time series in Fig. 5 is from the GNSS data repository of the Centro Sismologico Nacional, Chile (http://gps.csn.uchile.cl/data/). Basemaps in Fig. 2 are from Google Earth version 7.3.1 (https://earth.google.com, image copyright DigitalGlobe 2018) and Bing Maps (https://www.bing.com/maps, image copyright Earthstar Geographics SIO 2018). Fig. 7 uses SRTM data (USGS, 2004) downloaded using the USGS EarthExplorer (https://earthexplorer.usgs.gov/). Fig. 1 was drawn with the Generic Mapping Tools (Wessel et al., 2013). All coralline algae data are provided in the appendix.

Acknowledgements

This work was supported by the Natural Environment Research Council [NE/R00210X/1] with additional funding from the Department of Geography, Durham University. EG is funded by the European Union/Durham University (COFUND). We acknowledge financial support from the Millennium Nucleus CYCLO "The Seismic Cycle Along Subduction Zones" funded by the Millennium Scientific Initiative (ICM) of the Chilean Government grant NC160025 and Chilean National Fund for Development of Science and Technology (FONDECYT) grants 1150321 and 1181479. We thank Joaquim Otero for his help in the field, Dietrich Lange for providing his fault slip model and Ian Shennan for comments on the manuscript. We thank Aron Meltzner, an

anonymous reviewer and the Associate Editor, Nicola Litchfield, for comments that improved the paper. This is a contribution to IGCP project 639.

References

Adey, W.H., and I.G. Macintyre (1973). Crustose coralline algae: a re-evaluation in the geological sciences. Geol. Soc. Am. Bull. **84** 883–904.

Angermann, D., J. Klotz, and C. Reigber (1999). Space-geodetic estimation of the Nazca-South America Euler vector. Earth Planet. Sci. Lett. **171** 329–334.

Awata, Y., S. Toda, H. Kaneda, T. Azuma, H. Horikawa, M. Shishikura, T. Echigo. (2008). Coastal deformation associated with the 2007 Noto Hanto earthquake, central Japan, estimated from uplifted and subsided intertidal organisms. Earth Planets Space **60** 1059-1062.

Bedford, J. and M. Bevis. 2018. Greedy Automatic Signal Decomposition and Its Application to Daily GPS Time Series. J. Geophys. Res. Solid Earth **123** B014765

Béjar-Pizarro, M., D. Carrizo, A. Socquet, R. Armijo, S. Barrientos, F. Bondoux, S. Bonvalot, J. Campos, D. Comte, and J.B. De Chabalier. (2010). Asperities and barriers on the seismogenic zone in North Chile: state-of-the-art after the 2007 M w 7.7 Tocopilla earthquake inferred by GPS and InSAR data. Geophys. J. Int. **183** 390–406.

Bodin, P. and T. Klinger (1986). Coastal uplift and mortality of intertidal organisms caused by the September 1985 Mexico earthquakes. Science **233** 1071–1073.

Carver, G.A., A.S. Jayko, D.W. Valentine, and W.H. Li (1994). Coastal uplift associated with the 1992 Cape Mendocino earthquake, northern California. Geology **22** 195–198.

Castilla, J.C., P.H. Manríquez, and A. Camaño (2010). Effects of rocky shore coseismic uplift and the 2010 Chilean mega-earthquake on intertidal biomarker species. Mar. Ecol. Prog. Ser. **418** 17–23.

Clark, K.J., E.K. Nissen, J.D. Howarth, I.J. Hamling, J.J. Mountjoy, W.F. Ries, K., Jones, S. Goldstien, U. Cochran, and P. Villamor (2017). Highly variable coastal deformation in the 2016 Mw7. 8 Kaikōura earthquake reflects rupture complexity along a transpressional plate boundary. Earth Planet. Sci. Lett. **474**, 334–344.

Darwin, C. (1851). *Geological observations on coral reefs, volcanic islands, and on South America: Being the geology of the voyage of the Beagle, under the command of Captain Fitzroy, RN, during the years 1832 to 1836*, Smith, Elder and Co., London.

Duhart, P., and A.C. Adriasola (2008). New time-constraints on provenance, metamorphism and exhumation of the Bahía Mansa Metamorphic Complex on the Main Chiloé Island, south-central Chile. Andean Geol. **35** 79–104.

Egbert, G.D., and S.Y. Erofeeva (2002). Efficient inverse modeling of barotropic ocean tides. J. Atmos. Ocean. Technol. **19** 183–204.

Farías, M., G. Vargas, A. Tassara, S. Carretier, S. Baize, D. Melnick, and K. Bataille (2010). Land-level changes produced by the Mw 8.8 2010 Chilean earthquake. Science **329** 916.

FitzRoy, R. (1839). Narrative of the surveying voyages of His Majesty's Ships Adventure and Beagle between the years 1826 and 1836: describing their examination of the southern shores of South America, and the Beagle's circumnavigation of the globe. Henry Colburn., London.

Haeussler, P.J., R.C. Witter, and K. Wang (2015). Intertidal Biological Indicators of Coseismic Subsidence during the M_w 7.8 Haida Gwaii, Canada, Earthquake. Bull. Seismol. Soc. Am. **105** 1265–1279.

Jaramillo, E., Dugan, J.E., Hubbard, D.M., Melnick, D., Manzano, M., Duarte, C., Campos, C., Sanchez, R., (2012). Ecological implications of extreme events: footprints of the 2010 earthquake along the Chilean coast. PLoS One **7** e35348.

Jaramillo, E., Melnick, D., Baez, J.C., Montecino, H., Lagos, N.A., Acuña, E., Manzano, M., Camus, P.A., (2017). Calibrating coseismic coastal land-level changes during the 2014 Iquique (Mw= 8.2) earthquake (northern Chile) with leveling, GPS and intertidal biota. PLoS One **12** e0174348.

Kaye, C.A. (1964). The upper limit of barnacles as an index of sea-level change on the New England coast during the past 100 years. J. Geol. **72** 580–600.

Laborel, J., and F. Laborel-Deguen (1996). Biological indicators of Holocene sea-level and climatic variations on rocky coasts of tropical and subtropical regions. Quat. Int. **31** 53–60.

Laborel, J. (2005). Algal rims, in *Encyclopedia of Coastal Science* M. Schwartz (Editor), Wiley, New York, 24–25.

Lagabrielle, Y., B. Pelletier, G. Cabioch, M. Régnier, and S. Calmant (2003). Coseismic and long-term vertical displacement due to back arc shortening, central Vanuatu: Offshore and onshore data following the Mw 7.5, 26 November 1999 Ambrym earthquake. J. Geophys. Res. Solid Earth **108** B11 2519.

449 Lange, D., J. Ruiz, S. Carrasco, and P. Manríquez (2017). The Chiloé Mw 7.6 earthquake of 25
450 December 2016 in Southern Chile and its relation to the Mw 9.5 1960 Valdivia earthquake.
451 Geophys. J. Int. **213** 210-221.
452 Lay, T., H. Kanamori, C.J. Ammon, K.D. Koper, A.R Hutko, L. Ye, H. Yue, and T.M Rushing (2012).
453 Depth-varying rupture properties of subduction zone megathrust faults. J. Geophys. Res.
454 Solid Earth **117** B04311
455 Lemoine, P. (1913). Mélobésiées, in *Deuxième Expédition Antarctique Française (1908–1910)*
456 Anon (Editor), Masson and Cie, Paris, 1-67.
457 Lemoine, P. (1920). Botanische Ergebnisse der schwedischen Expedition nach Patagonien und
458 dem Feuerlande 1907-1909. VII. Melobésiés. K. Sven. Vetenskapsakademiens Handl. **61** 1–
459 17.
460 Martone, P.T., M. Alyono, and S. Stites (2010). Bleaching of an intertidal coralline alga:
461 untangling the effects of light, temperature, and desiccation. Mar. Ecol. Prog. Ser. **416** 57–
462 67.
463 Melgar, D., S. Riquelme, X. Xu, J.C. Baez, J. Geng, and M. Moreno (2017). The first since 1960: A
464 large event in the Valdivia segment of the Chilean Subduction Zone, the 2016 M7. 6
465 Melinka earthquake. Earth Planet. Sci. Lett. **474** 68–75.
466 Melnick, D., M. Cisternas, M. Moreno, and R. Norambuena (2012). Estimating coseismic coastal
467 uplift with an intertidal mussel: calibration for the 2010 Maule Chile earthquake (Mw=
468 8.8). Quat. Sci. Rev. **42** 29–42.

469 Melnick, D., S. Li, M. Moreno, M. Cisternas, J. Jara-Muñoz, R. Wesson, A. Nelson, J.C. Báez, and
470 Z. Deng. In Press. Back to full interseismic plate locking decades after the giant 1960 Chile
471 earthquake. Nat. Commun. DOI: 10.1038/s41467-018-05989-6
472 Melnick, D., M. Moreno, J. Quinteros, J.C. Baez, Z. Deng, S. Li, and O. Oncken (2017). The super-
473 interseismic phase of the megathrust earthquake cycle in Chile. Geophys. Res. Lett. **44**
474 784–791.
475 Meltzner, A.J., K. Sieh, H. Chiang, C. Shen, B.W. Suwargadi, D.H. Natawidjaja, B.E. Philibosian,
476 R.W. Briggs, and J. Galetzka (2010). Coral evidence for earthquake recurrence and an AD
477 1390–1455 cluster at the south end of the 2004 Aceh–Andaman rupture. J. Geophys. Res.
478 Solid Earth **115** B10402.
479 Meneses, I.C. (1993). Vertical distribution of coralline algae in the rocky intertidal of northern
480 Chile, in *Proceedings of the Fourteenth International Seaweed Symposium* A.R.O Chapman,
481 M.T. Brown and M. Lahaye (Editors) Springer, Dordrecht, 121–129.
482 Moreno, M., S. Li, D. Melnick, J.R. Bedford, J.C. Baez, M. Motagh, S. Metzger, S. Vajedian, C.
483 Sippl, and B.D. Gutknecht (2018). Chilean megathrust earthquake recurrence linked to
484 frictional contrast at depth. Nat. Geosci. **11** 285.
485 Moreno, M., D. Melnick, M. Rosenau, J.C. Baez, J. Klotz, O. Oncken, A. Tassara, J. Chen, K.
486 Bataille, and M. Bevis (2012). Toward understanding tectonic control on the Mw 8.8 2010
487 Maule Chile earthquake. Earth Planet. Sci. Lett. **321** 152–165.
488 Moreno, M., D. Melnick, M. Rosenau, J. Bolte, J. Klotz, H. Echtler, J.C. Baez, K. Bataille, J. Chen,
489 and M. Bevis (2011). Heterogeneous plate locking in the South–Central Chile subduction
490 zone: Building up the next great earthquake. Earth Planet. Sci. Lett. **305** 413–424.

Moreno, M.S., J. Bolte, J. Klotz, and D. Melnick (2009). Impact of megathrust geometry on inversion of coseismic slip from geodetic data: Application to the 1960 Chile earthquake. Geophys. Res. Lett. **36** L16310.

Munoz, J., R. Troncoso, P. Duhart, P. Crignola, L. Farmer, and C.R. Stern (2000). The relation of the mid-Tertiary coastal magmatic belt in south-central Chile to the late Oligocene increase in plate convergence rate. Rev. Geológica Chile **27** 177–203.

Nelson, A.R. (2007). Tectonic Locations, in *Encylopedia of Quaternary Science* S.A. Elias (Editor), Elsevier, Amsterdam, 3072–3087.

Ortlieb, L., S. Barrientos, and N. Guzman (1996). Coseismic coastal uplift and coralline algae record in northern Chile: the 1995 Antofagasta earthquake case. Quat. Sci. Rev. **15** 949–960.

Plafker, G. (1965). Tectonic deformation associated with the 1964 Alaska Earthquake. Science **148** 1675-1687.

Plafker, G. (1969). *Tectonics of the March 27, 1964, Alaska earthquake*. US Government Printing Office Washington, DC.

Plafker, G., and J.C. Savage (1970). Mechanism of the Chilean earthquakes of May 21 and 22, 1960. Geol. Soc. Am. Bull. **81** 1001–1030.

Plafker, G., and S.N. Ward, (1992). Back-arc thrust faulting and tectonic uplift along the Caribbean Sea coast during the April 22, 1991, Costa Rica earthquake. Tectonics **11** 709-718.

Ramirez-Herrera, M.-T., and J.J.Z. Orozco (2002). Coastal uplift and mortality of coralline algae caused by a 6.3 Mw earthquake, Oaxaca, Mexico. J. Coast. Res. **18** 75–81.

513 Rovere, A., Antonioli, F., Bianchi, C.N., 2015. Fixed biological indicators, in *Handbook of Sea-*
514 *Level Research* I Shennan, A.J. Long and B.P. Horton (Editors), Wiley, New Jersey, 268–280.
515 Ruiz, S., Moreno, M., Melnick, D., Campo, F., Poli, P., Baez, J.C., Leyton, F., Madariaga, R., 2017.
516 Reawakening of large earthquakes in South-Central Chile: The 2016 Mw7. 6 Chiloé event.
517 Geophys. Res. Lett. 44, 6633–6640.
518 Shennan, I., E. Garrett, and N. Barlow (2016). Detection limits of tidal-wetland sequences to
519 identify variable rupture modes of megathrust earthquakes. Quat. Sci. Rev. **150** 1–30.
520 Tarr, R.S., and L. Martin (1912). The earthquakes at Yakutat Bay, Alaska, in September, 1899.
521 Bull. Seis. Soc. Am. **2** 254-255.
522 Thatcher, W. (1984). The earthquake deformation cycle at the Nankai Trough, southwest Japan.
523 J. Geophys. Res. Solid Earth **89** 3087–3101.
524 United States Geological Survey (2004). Shuttle Radar Topography Mission, 1 Arc Second scenes
525 s44_w075, s44_w074, s43_w075 and s43_074, Unfilled Unfinished 2.0, Global Land Cover
526 Facility, University of Maryland, College Park, Maryland, February 2000.
527 Vargas, G., M. Farías, S. Carretier, A. Tassara, S. Baize, and D. Melnick (2011). Coastal uplift and
528 tsunami effects associated to the 2010 Mw8. 8 Maule earthquake in Central Chile. Andean
529 Geol. **38** 219-238.
530 Velásquez, C., E. Jaramillo, P.A. Camus, M. Manzano, and R. Sánchez (2016). Biota del
531 intermareal rocoso expuesto de la Isla Grande de Chiloé, Archipiélago de Chiloé, Chile:
532 Patrones de diversidad e implicancias ecológicas y biogeográficas. Rev. Biol. Mar.
533 Oceanogr. **51** 33–50.

534 Xu, W., 2017. Finite-fault Slip Model of the 2016 Mw 7.5 Chiloé Earthquake, Southern Chile,
535 Estimated from Sentinel-1 Data. Geophys. Res. Lett. 44, 4774–4780.

Mailing addresses

Ed Garrett, Department of Geography, Durham University, South Road, Durham, DH1 3LE, UK

Martin Brader, Department of Geography, Durham University, South Road, Durham, DH1 3LE, UK

Daniel Melnick, Instituto de Ciencias de la Tierra, Universidad Austral de Chile, Edificio Emilio Pugín, Avenida Eduardo Morales Miranda, Campus Isla Teja, Valdivia, Chile

Jonathan Bedford, GFZ German Research Centre for Geosciences, Telegrafenberg, Building C, 14473 Potsdam, Germany

Diego Aedo, Instituto de Ciencias de la Tierra, Universidad Austral de Chile, Edificio Emilio Pugín, Avenida Eduardo Morales Miranda, Campus Isla Teja, Valdivia, Chile

Tables

Table 1: Summary of coralline algae survey data. See Appendix table A1 for complete dataset.

Location	Site #	Latitude	Longitude	Number of measurements	Mean VEM (cm)	Standard deviation (cm)	Mean aspect (°)	Degree of wave exposure	Notes
Isla Quilán/Isla Refugio	1	-43.41894	-74.25331	40	27.4	6.8	31	Sheltered	
	2	-43.41714	-74.25099	15	25.1	6.6	59	Sheltered	
	3a	-43.41095	-74.24069	-	-	-	170	Moderate	No bleaching observed
	3b	-43.41081	-74.24061	-	-	-	130	Sheltered	Bleaching evident but la vertical bedrock
	3c	-43.40992	-74.23958	-	-	-	270	Sheltered	Bleaching evident but la vertical bedrock
	4	-43.42138	-74.24784	26	25.3	7.5	352	Sheltered	
	5	-43.42107	-74.25425	3	28.7	10.7	227	Sheltered	Poorly-defined growth l most areas
	6	-43.42155	-74.25694	19	23.3	7.1	35	Sheltered	
	7	-43.42225	-74.25701	-	-	-	140	Sheltered	Lacking clearly identifia algae
	8	-43.42325	-74.25905	-	-	-	230	Sheltered	Bleaching evident but la vertical bedrock
	9	-43.41234	-74.24683	-	-	-	190	Moderate	No bleaching observed
	10	-43.41834	-74.25217	-	-	-	250	Sheltered	Bleaching evident but la vertical bedrock
	Total			103	25.8	7.14			
Punta Rocosa, Isla de Chiloé	11	-43.36237	-74.13142	-	-	-	200	Moderate	No bleaching observed, defined living limit
	12	-43.36757	-74.13046	-	-	-	160	High	No bleaching observed
	13	-43.36760	-74.12961	-	-	-	140	High	No bleaching observed, defined living limit

Figures

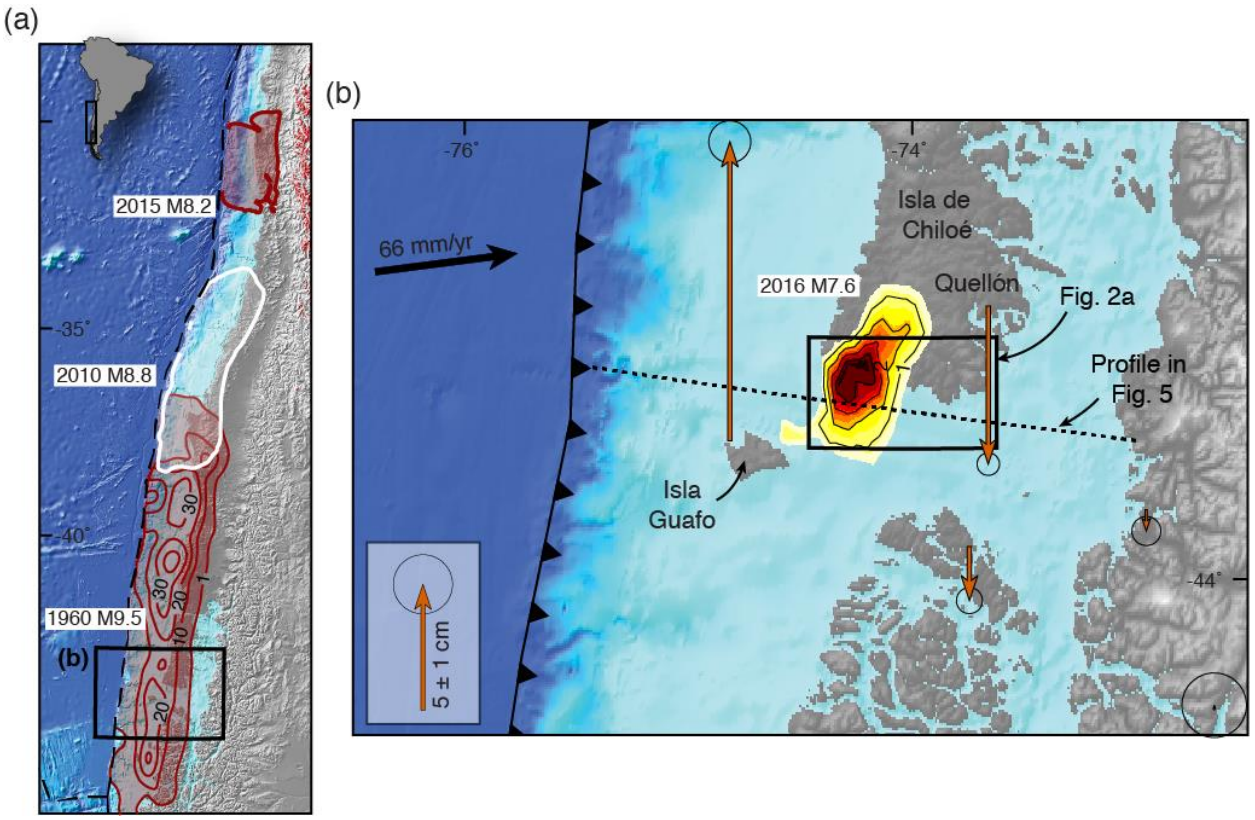

Figure 1: The regional context of the 2016 Chiloé earthquake. a) The Chilean megathrust, including the slip distribution of the 1960 Valdivia earthquake, with contours in meters (Moreno et al., 2009), and the location of the 2010 Maule and 2015 Illapel earthquakes. b) The 2016 Chiloé earthquake, including coseismic vertical GPS offsets (arrows) and slip distribution in meters inferred from space-based geodesy (Moreno et al., 2018).

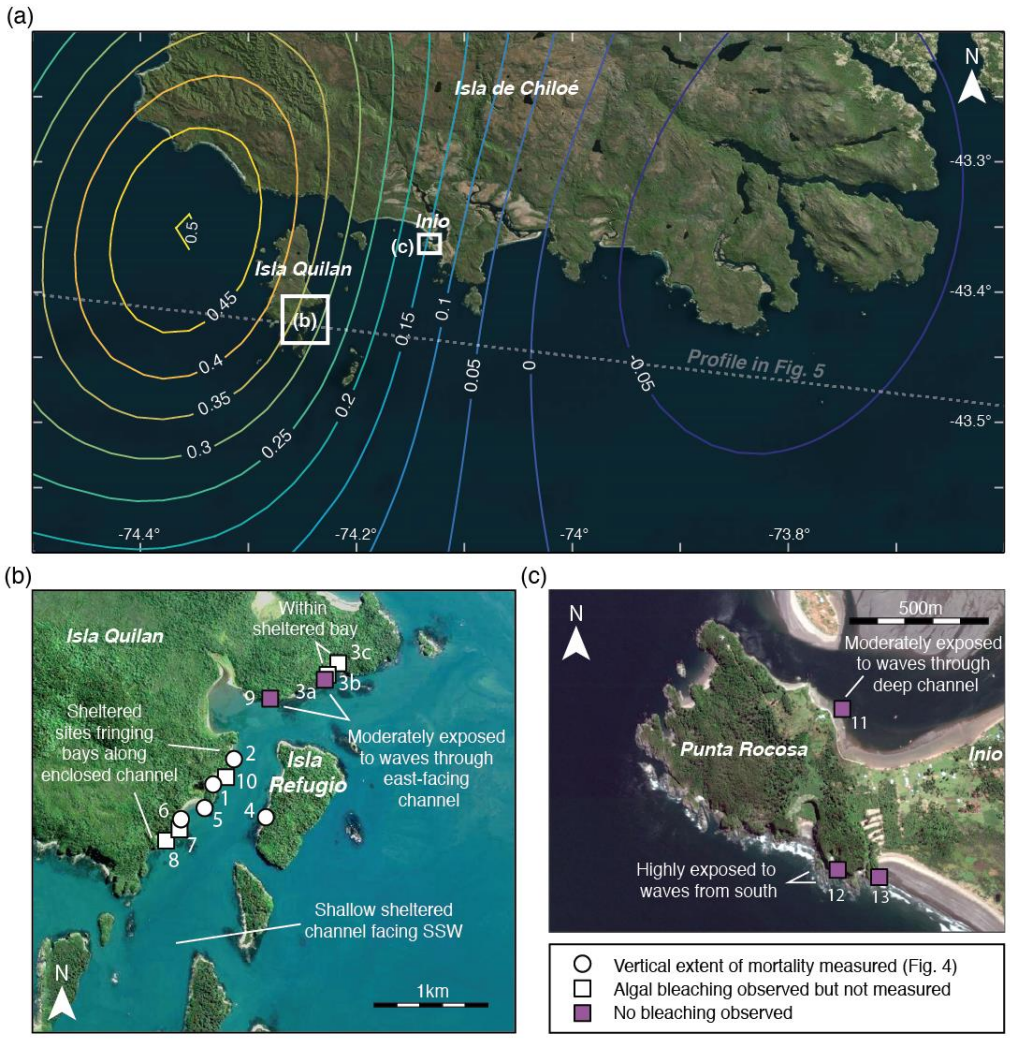

558

559 Figure 2: Field survey locations. a) The southern coast of Isla de Chiloé and outlying islands.
560 Contours indicate forward modeled coseismic vertical land-level change in 2016 resulting from
561 Moreno et al.'s (2018) inferred slip distribution. Contours are at 0.05 m intervals, with uplift
562 positive. b) Coralline algae survey sites on the southeastern coast of Isla Quilán and the western
563 coast of Isla Refugio. c) Coralline algae survey sites around Punta Rocosa.

564

565 Figure 3: Field photographs of coralline algae survey sites on a-e) Isla Quilán and f) Punta
566 Rocosa. a, b) Conspicuous uplifted and bleached algae at sites 1 and 2. c) Living algae at site 5 in
567 an area with predominantly poorly defined growth limits. d) Site 3a, with no evidence of algal
568 bleaching. e) Site 3b, displaying bleaching on mobile substrates and bedrock approximately

569 20 m from site 3a, but lacking vertically inclined surfaces suitable for VEM measurement. f)
570 Living algae at site 13 in an area of low surface coverage and poorly defined upper growth
571 limits.

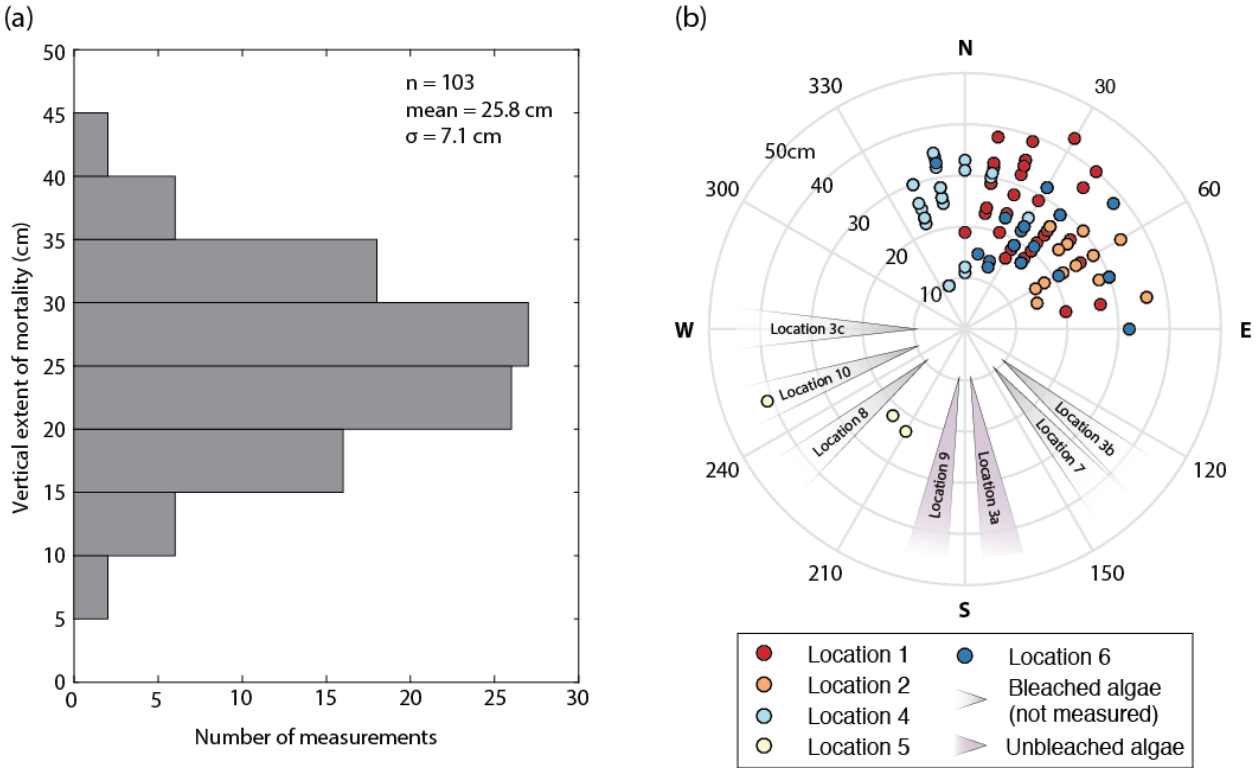

572

573 Figure 4: a) Vertical extent of coralline algae mortality at Isla Quilán. b) Rose diagram showing
574 the aspect of sites with VEM measurements or observations of the presence or absence of
575 bleaching.

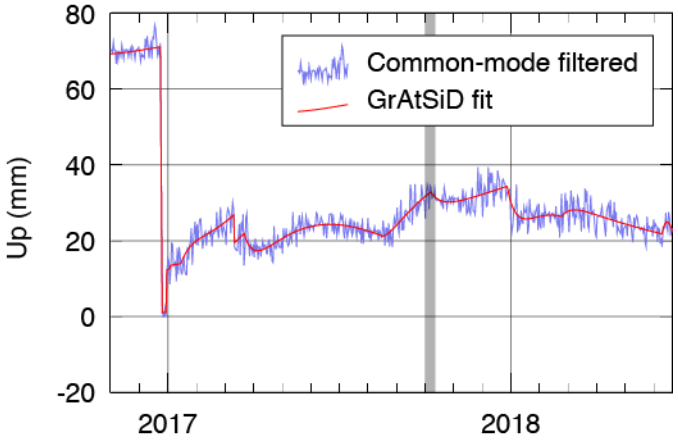

576

577 Figure 5: Coseismic and postseismic vertical displacements recorded by GPS station QLLN at
578 Quellón (see Fig. 1b for location). We apply a common mode filter and model the time series
579 with the GrAtSiD algorithm (Bedford and Bevis, 2018). The vertical bar indicates the timing of
580 our VEM measurements at Isla Quilán in October 2017

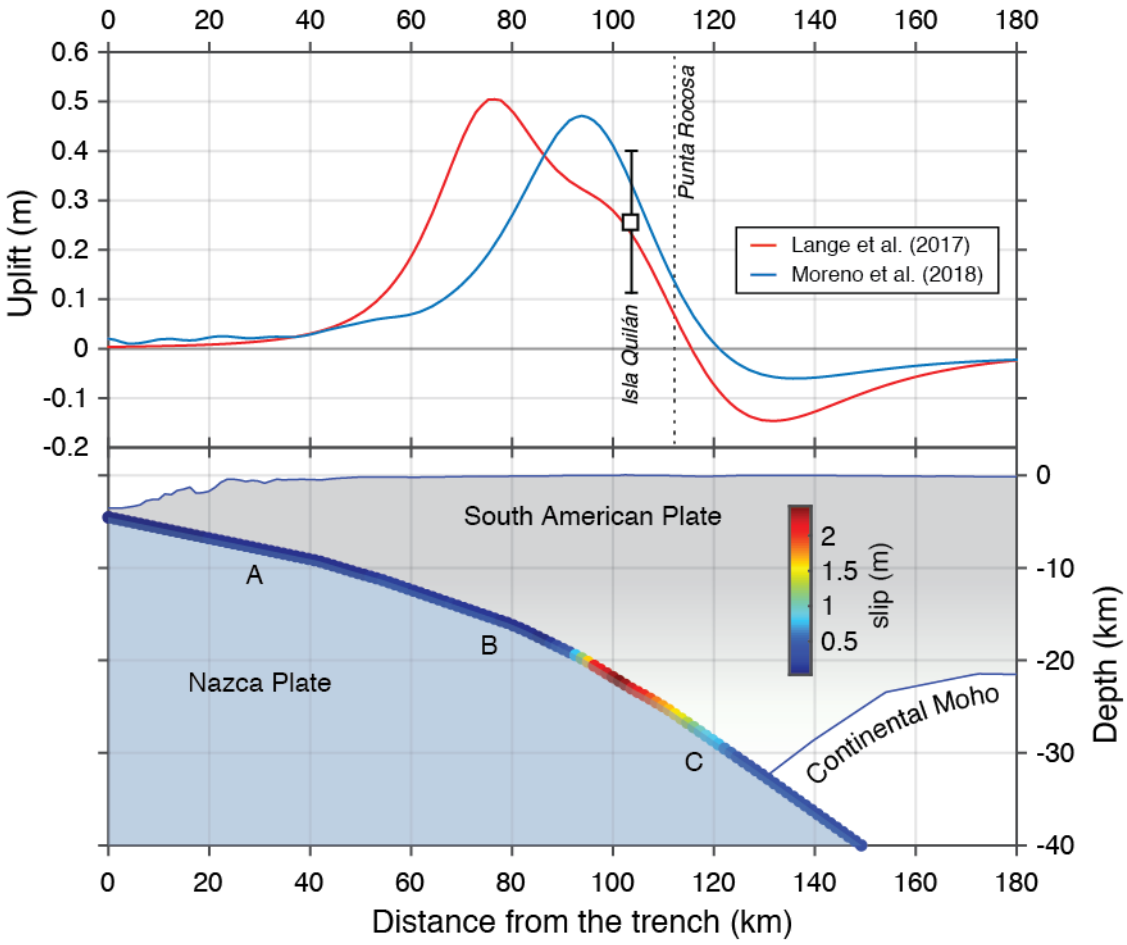

581

582 Figure 6: Predicted surface deformation (upper panel) resulting from Lange et al. (2017) and
583 Moreno et al. (2018) slip distributions along the transect shown in Fig. 1. Black box and
584 whiskers represent uplift at Isla Quilán (VEM mean ±2σ). Both slip distributions use the fault
585 geometry of Moreno et al. (2018), as shown in the lower panel. The lower panel also depicts
586 Moreno et al.'s (2018) slip distribution along the transect. Letters A, B and C locate seismogenic
587 failure domains (following Lay et al., 2012).

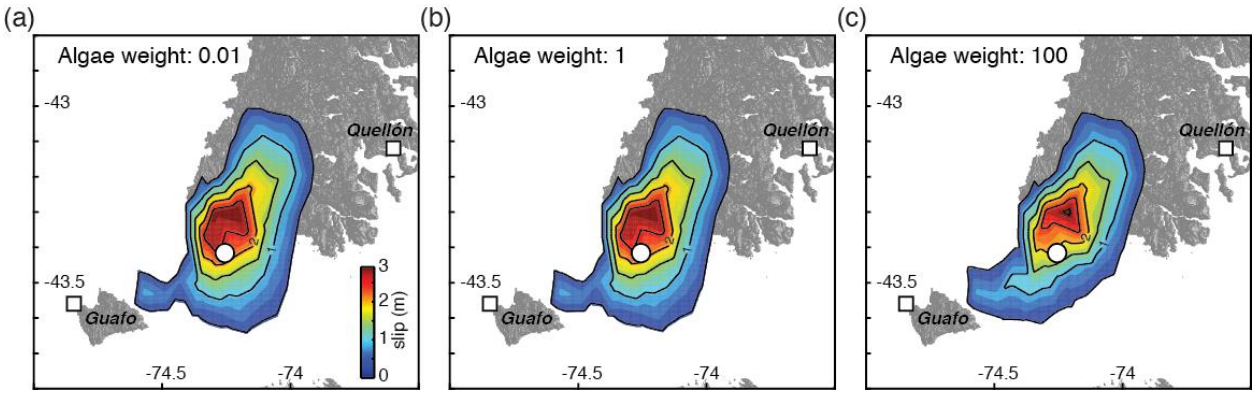

588

589 Figure 7: Impact of including the Isla Quilán uplift estimate (white circle) on the modeled
590 distribution of coseismic fault slip in 2016. Initial model specifications are provided by Moreno
591 et al. (2018), with the additional coralline algae constraint weighted at ratios of a) 0.01:1 b) 1:1
592 or c) 100:1 with respect to the combined GPS and InSAR data. White squares are GPS stations at
593 Quellón and Guafo.

Appendices

Table A1: Vertical extent of coralline algae mortality and corresponding bedrock surface aspect for each measurement point on Isla Quilán or Isla Refugio. See table 1 for data summary and Figure 2b for site locations.

SIte	VEM (cm)	Aspect (°)
1	39	20
1	29	10
1	23	10
1	32	10
1	19	0
1	26	60
1	28	20
1	34	20
1	35	20
1	38	10
1	26	40
1	29	10
1	43	30
1	29	40
1	40	40
1	35	20
1	18	40
1	20	40
1	24	40
1	24	20
1	25	40
1	18	30
1	26	50
1	27	80
1	32	20
1	33	10
1	17	40
1	29	30
1	26	40
1	34	20
1	36	40
1	22	20
1	22	40
1	24	40
1	24	10
1	20	40
1	25	40
1	16	30
1	20	80
1	27	50
2	36	80

2	35	60
2	30	70
2	28	70
2	25	60
2	26	50
2	29	60
2	30	50
2	22	60
2	18	60
2	16	60
2	17	40
2	24	50
2	26	40
2	15	70
4	25	350
4	23	340
4	32	30
4	30	340
4	32	350
4	22	340
4	26	350
4	30	10
4	33	0
4	34	350
4	23	340
4	9	340
4	11	0
4	35	350
4	25	340
4	25	30
4	30	340
4	28	350
4	26	340
4	26	350
4	31	10
4	31	0
4	28	350
4	23	340
4	9	340
4	12	0
5	22	220
5	41	250
5	23	210
6	32	90
6	30	70
6	38	50
6	22	30
6	32	30
6	17	40
6	29	40

6	23	20
6	21	60
6	19	30
6	21	40
6	19	30
6	23	30
6	19	30
6	15	10
6	33	350
6	14	20
6	23	30
6	13	20

598